

Ultrathin Polydopamine Films with Phospholipid Nanodiscs Containing a Glycophorin A Domain

Tommaso Marchesi D'Alvise, Sean Harvey, Lisa Hueske, Jolanta Szelwicka, Lothar Veith, Tuomas P. J. Knowles, Dennis Kubiczek, Carolin Flaig, Fabian Port, Kay-E. Gottschalk, Frank Rosenau, Bartłomiej Graczykowski, George Fytas, Francesco S. Ruggeri, Katrin Wunderlich,* and Tanja Weil*

Cellular membranes have long served as an inspiration for nanomaterial research. The preparation of ultrathin polydopamine (PDA) films with integrated protein pores containing phospholipids and an embedded domain of a membrane protein glycophorin A as simplified cell membrane mimics is reported. Large area, ultrathin PDA films are obtained by electropolymerization on gold surfaces with 10–18 nm thickness and dimensions of up to 2.5 cm². The films are transferred from gold to various other substrates such as nylon mesh, silicon, or substrates containing holes in the micrometer range, and they remain intact even after transfer. The novel transfer technique gives access to freestanding PDA films that remain stable even at the air interfaces with elastic moduli of ≈6–12 GPa, which are higher than any other PDA films reported before. As the PDA film thickness is within the range of cellular membranes, monodisperse protein nanopores, so-called “nanodiscs,” are integrated as functional entities. These nanodisc-containing PDA films can serve as semi-permeable films, in which the embedded pores control material transport. In the future, these simplified cell membrane mimics may offer structural investigations of the embedded membrane proteins to receive an improved understanding of protein-mediated transport processes in cellular membranes.


great selectivity. Proteins serve as important components of cellular membranes that impart functionality and ligand-specificity thus regulating, for example, many transport processes^[1] or bioenergy production.^[2] There has been much interest in the fabrication of synthetic cell membrane mimics with comparable properties, and different materials have been considered including lipid bilayers,^[3] block copolymer membranes,^[4] vesicles,^[5] synthetic channels,^[6] or nanoporous membranes.^[7] Distinct nanosized objects such as phospholipid nanodiscs with inner lipid bilayers also provide certain properties of cellular membranes. Thus, host membrane proteins could be embedded that retain their structure integrity and functionality.^[8,9] Nanodiscs consist of self-assembled lipid bilayers encircled by two amphipathic membrane scaffold proteins (MSP) leading to a discoidal structure with varying diameters from ≈8 to 17 nm.^[10]

It would be desirable to generate ultrathin polymeric films with thicknesses comparable to lipid bilayer membrane ranging from 5 to 8 nm^[11] containing nanodiscs that could host membrane proteins. However, the preparation of ultrathin and stable polymeric films with such

1. Introduction

Nature has evolved cellular membranes with various remarkable features to control material transport within cells with

T. Marchesi D'Alvise, Dr. S. Harvey, L. Hueske, J. Szelwicka, Dr. L. Veith, Dr. B. Graczykowski, Prof. G. Fytas, Dr. K. Wunderlich, Prof. T. Weil
Max Planck Institute for Polymer Research
Ackermannweg 10, Mainz 55128, Germany
E-mail: wunderlich@mpip-mainz.mpg.de; weil@mpip-mainz.mpg.de
Prof. T. P. J. Knowles, Dr. F. S. Ruggeri
Centre for Misfolding Diseases
Department of Chemistry
University of Cambridge
Cambridge CB2 1EW, UK

 The ORCID identification number(s) for the author(s) of this article can be found under <https://doi.org/10.1002/adfm.202000378>.

© 2020 The Authors. Published by WILEY-VCH Verlag GmbH & Co. KGaA, Weinheim. This is an open access article under the terms of the Creative Commons Attribution License, which permits use, distribution and reproduction in any medium, provided the original work is properly cited.

Dr. D. Kubiczek, Dr. F. Rosenau
Institute for Pharmaceutical Biotechnology
Ulm University
Albert-Einstein-Allee 11, Ulm 89081, Germany
C. Flaig, F. Port, Prof. K.-E. Gottschalk
Institute for Experimental Physics
Ulm University
Albert-Einstein-Allee 11, Ulm 89081, Germany
Dr. B. Graczykowski
Faculty of Physics
Adam Mickiewicz University
Uniwersytetu Poznańskiego 2, Poznań 61-614, Poland

DOI: 10.1002/adfm.202000378

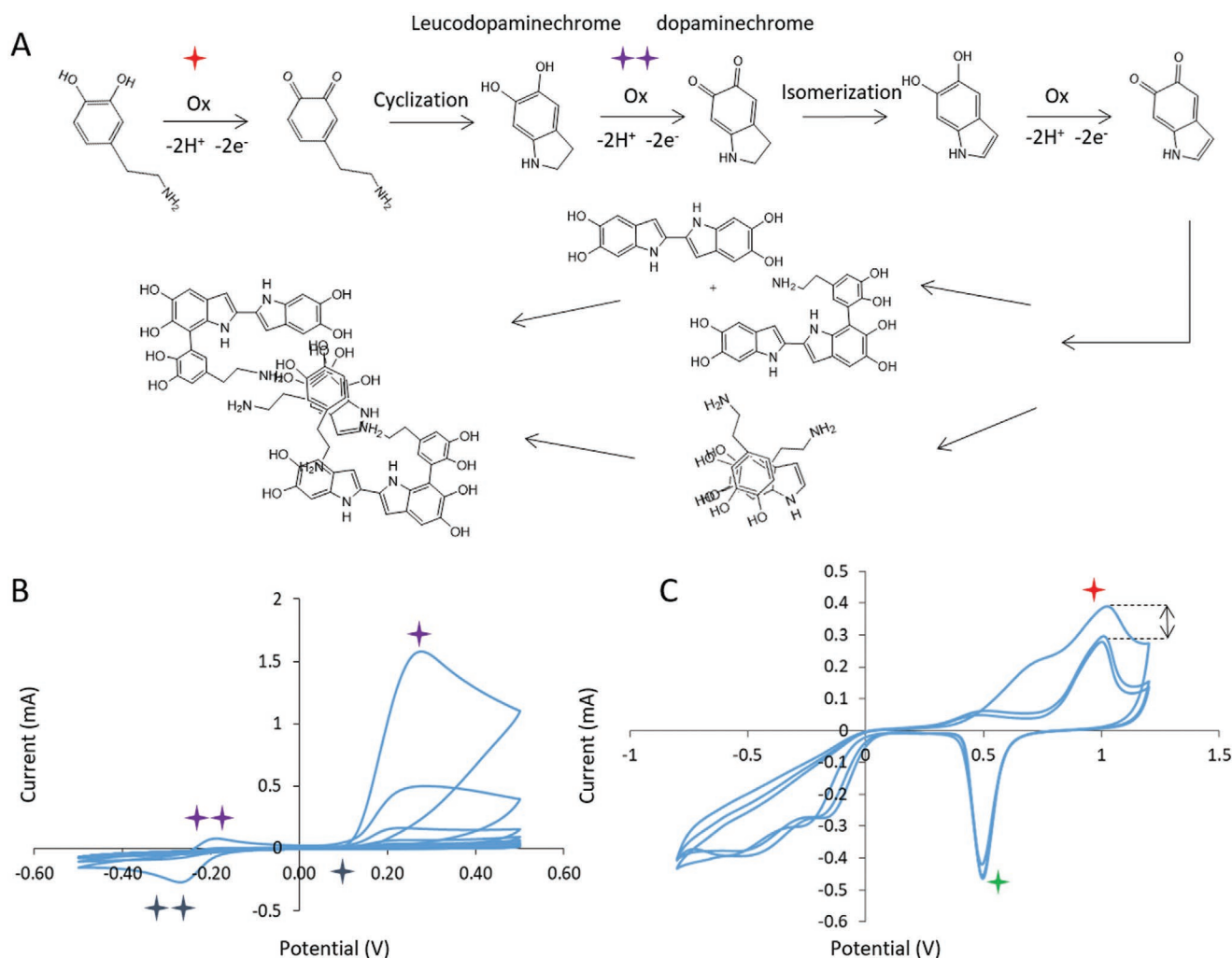


Figure 1. A) PDA polymerization. The first oxidations steps are also present in the electropolymerization (violet stars) representing the starting reaction for PDA formation. The highly cross-linked PDA is obtained by covalent bonds and supramolecular interactions. B) Typical cyclic voltammogram of PDA electropolymerization on gold. The potential is sweep between -0.5 and $+0.5$ V with a scan rate of 0.01 V s^{-1} using a gold counter electrode and an Ag/AgCl reference electrode. The typical catechol to quinone oxidation peak, observed at ≈ 0.3 V (violet star), the second oxidation peak (two violet stars) is present -0.2 V. The reduction peaks are assigned at 0.15 and -0.3 V (one and two blue stars, respectively). The peak intensity decreases over the cycles until it disappears in the fourth cycle, due to the deposition of the insulating PDA layer. C) Electrochemical removal procedure of PDA. All three curves show a cyclic voltammogram of gold with a typical gold oxidation peak at 1 V (red star) and the reduction at 0.5 V (green star). The decrease of current intensity (indicated with an arrow) from the first curve to the second one and the presence of a peak at 0.6 V, which afterward disappears, suggested reduced interactions between the PDA film and the gold substrate, hence further oxidation only arises from the gold surface.

dimensions is very challenging,^[12] and film transfer to other substrates^[13–15] without damage as well as the introduction of biological entities into such films still remains elusive. Polydopamine (PDA) is a highly cross-linked polymer formed by the oxidative polymerization of dopamine revealing several similarities to the naturally occurring biopolymers, melanins, and eumelanins.^[16] PDA (Figure 1A) is considered biocompatible, it is resistant to a number of reagents, highly adhesive to various materials and surfaces^[17] and hence, it has been used for functionalization of many substrates.^[18,19] There is a rich chemistry available, via which PDA surfaces could be functionalized, for example, with Schiff base reactions or Michael additions. Freestanding PDA films with a thickness of several hundreds of nanometers or even micrometers have been synthesized before.^[20–27] Ultrathin and homogeneous PDA films attached

to gold surfaces with thicknesses of 5 – 20 nm have been prepared by electropolymerization.^[28] Electropolymerization is considerably faster than the often applied dip coating procedure, allowing precise control of the film thickness and homogeneity.^[20,28–30] Although this mild polymerization technique is restricted to conductive materials, it provides the opportunity to embed non-conductive materials, for example, biomolecules into the PDA film. Until now, applying positive potentials for film removal after electropolymerization only resulted in delamination and destruction of the PDA films.^[31] To the best of our knowledge, electropolymerization has never been used to prepare ultrathin freestanding PDA films.

Herein, we present the electropolymerization of large area, ultrathin PDA films with 10 – 18 nm thickness and dimensions of up to 2.5 cm², exhibiting high elastic moduli (between 6 and

12 GPa) facilitating their transfer to various substrates. This approach also allowed the preparation and transfer of patterned PDA structures. Due to the PDA film thickness in the range of lipid bilayers, phospholipid nanodiscs were introduced into the PDA films containing the membrane domain of glycophorin A, an antigen-presenting membrane protein found at the surface of human erythrocytes.^[32] Such nanodisc-containing ultrathin PDA films offer potential for the selective separation of organic molecules, nanopore-based DNA-sequencing, cascade reactions, or sensing. We also envision that they could serve as very simplified cell membrane models offering structural investigations of the embedded membrane proteins or to study protein-mediated transport processes in cellular membranes.

2. Results and Discussion

2.1. Preparation of Ultrathin, Free-Standing PDA Films

Ultrathin PDA films were prepared on a gold substrate by cyclic voltammetry (CV) (Figure 1B) immersing the gold substrate in dopamine solution and sweeping the potential between -0.5 and $+0.5$ V for several cycles.^[28,33] In Figure 1A, a simplified representation of one of the possible mechanisms of polydopamine formation and structure is depicted. The first step is

the oxidation of catechol to quinone followed by cyclization and another oxidation step from leucodopaminechrome to dopaminechrome. Oxidative polymerization of dopaminechrome affords the highly cross-linked polydopamine film. Polydopamine growth and the chemical composition of the film was proven by IR spectroscopy (Figure S4, Supporting Information) and the chemical signature corresponded to previous reports.^[34] In order to remove the film, we adapted a method developed by Greco et al.,^[35] where a sacrificial polymeric layer, polyvinyl alcohol (PVA), was used as mechanical support for the removal of a poly(3,4-ethylenedioxythiophene) polystyrene sulfonate (PEDOT/PSS) nanofilm from the substrate as depicted in Figure 2A. Prior to removal, the PDA film at the gold surface was immersed into carbonate buffer at pH 10 for 30 min to allow further cross-linking of the dopamine monomers and oligomers absorbed into the film (Figure S1, Supporting Information), which renders the film more stable and compact and was essential to facilitate film removal (Figure 2A).^[36] The sample was then dipped into phosphate buffer and three additional cycles were applied over a wider potential range -800 to 1200 mV to overoxidize the system by forming an oxide layer on gold that reduces the adhesion between the film and the gold substrate.^[37] According to previous reports, this procedure reduces the Au–N coordination thus allowing detachment of the PDA film.^[38,39] Figure 1C

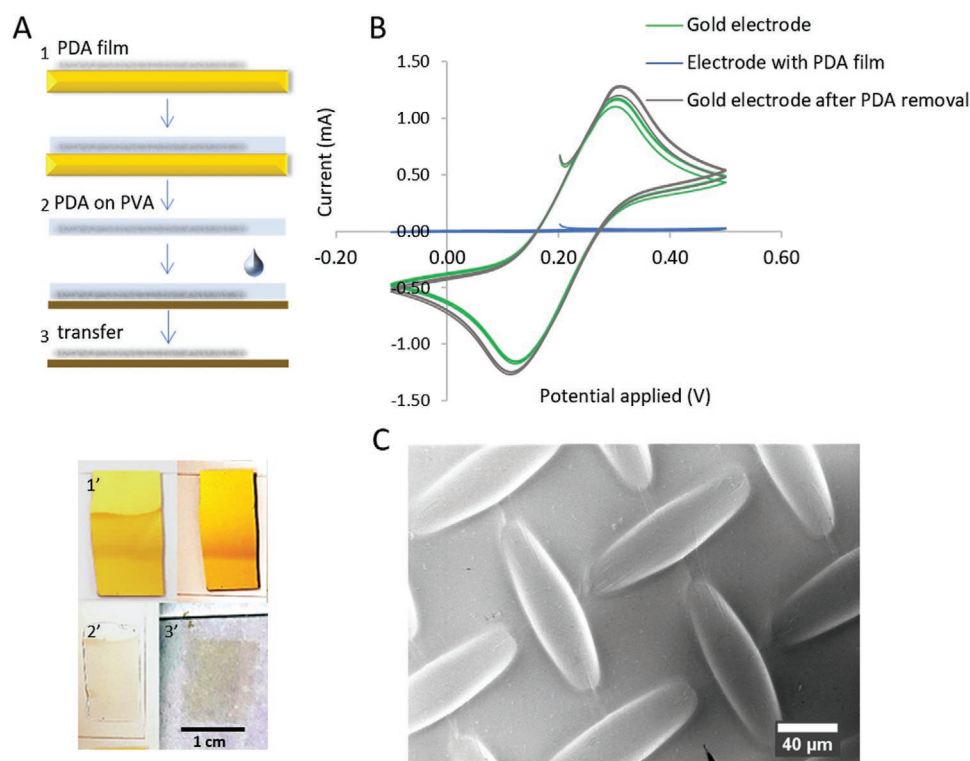


Figure 2. A) Top: Schematic procedure of the removal and transfer procedure of freestanding PDA films (gray) on gold substrate (yellow); three main steps are shown: 1) Formation of the PDA film, 2) Stripping of the PDA film off the gold substrate by applying PVA (light blue), 3) Transfer of the PDA film onto a different substrate (brown) by dissolving PVA with water. Bottom: Photos recorded of each sample during the corresponding procedure; 1') the PDA film on the gold substrate; 2') the removed PDA film on the transparent PVA support; 3') the PDA film transferred onto a glass slide by dissolving the PVA layer. B) Cyclic voltammetry (CV) curves recorded between -0.5 and $+0.5$ V of equimolar solutions of $5\text{ mM K}_3[\text{Fe}(\text{CN})_6]$ and $\text{K}_4[\text{Fe}(\text{CN})_6]$ for an uncoated gold electrode of $1 \times 1.5\text{ cm}$ (green curve) and the CV curve of the same electrode coated with the PDA film after 15 cycles at scan rate of 0.01 V s^{-1} (blue curve). The CV curve of the clean electrode after the removal of the PDA film (gray curve). C) SEM micrograph of a freestanding PDA film on a nylon mesh. The PDA film was obtained after 15 cycles by cyclic voltammetry with a thickness of $\approx 17\text{ nm}$ and covers the mesh homogeneously.

depicts the electrochemical removal cycles; at 1000 mV, the corresponding oxidation peak of gold is clearly present.

The peak intensity decreased after the first cycle due to over oxidation of the PDA film and the gold surface thus weakening the bonds between these two materials. Consequently, the following cycles revealed oxidation and reduction of bare gold indicating the reduced interactions of the PDA film and the gold surface. The area under the curve (AUC) of the oxidation and reduction peaks of gold (Table S1, Supporting Information) was calculated. A decrease of the AUC was observed after the first electrochemical cycle for the oxidation peak but all following AUC remained constant. No changes were detected for the AUC of the gold reduction peaks. Next, the PDA film was coated with a sacrificial PVA layer, which served as an adhesive tape and mechanical support for handling the ultrathin PDA film. The coating was performed by dropcasting of a PVA solution (200 μ L, 10%) in water and after drying the layer at 40 $^{\circ}$ C for approximately 25 min, the PDA film was stripped off the substrate together with the PVA film (Figure 2A). In the corresponding CV (Figure 2B), successful removal of the entire PDA film with the PVA layer was clearly visible. Thereafter, PVA was removed by immersing the PVA–PDA film in water to generate the freestanding PDA film (Figure S2, Supporting Information). Under these conditions, the $K_3[Fe(CN)_6]/K_4[Fe(CN)_6]$ redox couple was applied by three cycles of CV to demonstrate the complete removal of the PDA film from the gold substrate. The typical cyclic voltammogram of the gold surface with an oxidation peak at 0.4 V and a reduction peak at 0 V was recovered after the removal of the PDA film indicating that the gold was clean without residual PDA after this procedure (Figure 2B). The ultrathin PDA film at the air/water interface was then transferred to various substrates such as a nylon mesh and characterized by SEM (Figure 2C) to demonstrate its capability to stand freely without the need for another supporting material.

2.2. Chemical and Mechanical Characterization of Freestanding PDA Films

Following the previously described procedure, the PDA film was placed onto other supports such as silicon, which is attractive for conducting AFM measurements (Figure S3, Supporting Information), Si_3N_4 or gold. After direct transfer of the PVA–PDA film onto the respective substrate, the PVA layer was removed by a simple water wash. To elucidate whether residual PVA was present after the removal procedure, the films were transferred back onto the gold surface and infrared nanospectroscopy (AFM-IR) measurements were performed (Figure 3A). It is possible to use grazing-angle reflectance FTIR spectroscopy to obtain a spectrum of the PDA thin film on a reflective substrate like gold, but it becomes unprecise when measuring a transferred film due to the presence of wrinkles. Instead, the infrared nanospectroscopy technique combines the high spatial resolution of atomic force microscopy (AFM) with the chemical recognition power of Infrared (IR) spectroscopy.^[40,41] AFM-IR is thus capable to acquire and correlate simultaneously the morphological and chemical properties of thin films with 3–8 nm thickness with a spatial resolution in the order of the radius of the AFM probe (≈ 10 –20 nm).^[42,43] The PDA film electropolymerized on

gold appeared highly homogeneous (Figure 3A). After acquiring the three-dimensional morphology of the sample, nanoscale resolved IR spectra were acquired by AFM-IR between 1800 and 1250 cm^{-1} . The spectrum shows the typical broad IR absorption of PDA related to C–C aromatic ring vibrations at 1600 cm^{-1} and a weaker absorption of the C–O bond vibrations at approximately 1250 cm^{-1} . The nanoscale resolved spectra of the thin PDA layer were in excellent agreement with the IR spectrum of bulk PDA reported in the literature and from grazing-angle reflectance FTIR on thin films (Figure S4, Supporting Information) showing the same absorbance peak at 1600 and 1250 cm^{-1} . In the case of the transferred PDA film (Figure 3B), the surface did not appear as homogeneous as the freshly prepared film surface and the acquisition of the nanoscale morphology of the film revealed that some wrinkles were present probably due to swelling of the PVA layer during dissolution in water. In the AFM-IR localized spectra, the signal relating to residual PVA was detected at 1725 cm^{-1} and between 1280 and 1250 cm^{-1} corresponding to C=O and C–O bonds in the PVA, respectively (Figure 3B). It is very challenging to remove sacrificial polymers entirely^[44] most likely due to strong hydrogen bonds between PVA and PDA.^[45] Other polymers were also evaluated as sacrificial layers but PVA gave the best results most likely due to many non-covalent hydrogen-bond interactions with the PDA film.

To measure the elastic Young modulus (E) and residual stress (σ_0) of freestanding PDA films, we employed the contactless and non-invasive micro-Brillouin light spectroscopy (μ -BLS) at GHz frequencies^[46] (Figure S5, Supporting Information). An outstanding high E modulus between 10 and 12 GPa was obtained for PDA films that were fabricated after 5 and 10 CV cycles. The E modulus dropped to 6 GPa for the films prepared after 15 CV cycles (Figure 3C). This decrease could be due to the deposition of a less densely packed PDA layer after 10 cycles reducing the overall mechanical film properties.^[47] Prior studies of PDA films prepared by dip coating and measured by the compressive thin film buckling contact technique reported an elastic modulus of about 2 GPa for a film thickness of about 25 nm.^[31] The PDA films reported herein revealed much higher elastic moduli at lower thickness (10, 13, 16 nm) and the freestanding PDA films formed after 5 and 10 cycles show elastic moduli within the same range as carbon nanomembranes.^[48]

The enhanced elasticity made our film more suitable for self-supporting applications, where the stiffness of the material plays a critical role for the long-term stability of the film. However, residual PVA on the PDA film could still affect the elastic modulus and it was reported that elimination of sacrificial PVA layers could further enhance the failure strength of the freestanding film.^[49]

Next, we evaluated the possibility to polymerize dopamine only on conductive areas of the substrate and leave out non-conductive spaces. In this way, PDA formation could be controlled spatially, which provides access to ultrathin patterned PDA films. First, patterned PDA films were prepared on gold electrodes by masking the surface with polydimethylsiloxane (PDMS), which blocked the electron flow and allowed polymerization only at the PDMS-free areas as shown in Figure 3D. With this method, the word “MPIP” was written using letters patterned in PDMS. The PDA letters with heights of about 2.5 μ m and thicknesses of ≈ 17 nm were transferred onto a phosphorescent glass slide (Figure 3D) based on the

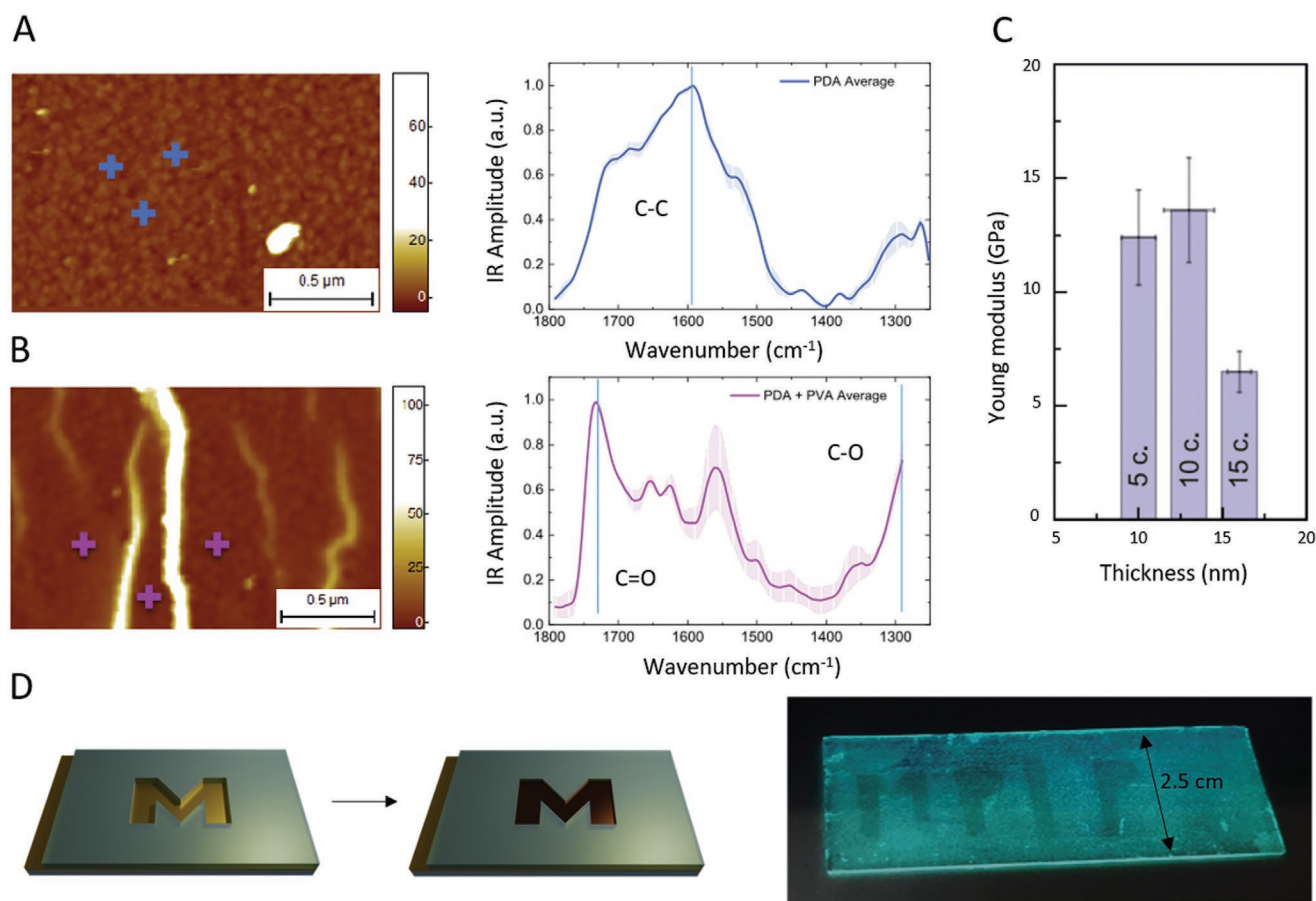


Figure 3. A,B) Correlation between the three-dimensional morphology (left) and nanoscale localized chemical spectra (right) of the PDA film acquired by AFM-IR at the locations indicated by the crosses. A) Electropolymerized PDA film on gold; B) PDA film on gold after removal of PDA and back-transfer. The three crosses in the AFM images indicate areas, where the corresponding IR spectra were acquired and averaged. C) Plot of the elastic modulus values (Table S3, Supporting Information) with thickness obtained for the PDA films prepared after 5, 10, and 15 CV cycles (5c, 10c, and 15c, respectively) transfer on Silicon (Table S2, Supporting Information). D) Schematic procedure for the preparation of a patterned PDA films applying a mask (right) taking the letter M as an example. The gold surface (yellow) was partly covered using a PDMS mask (gray). Electropolymerization proceeds only at the accessible, unmasked area of the gold surface, where the PDA film is able to form (brown). Left: Patterned PDA film with the shape of the letters MPIP (height: 2.5 cm) that was prepared and transferred onto a glass slide.

transfer protocol depicted in Figure 2A. The image shows that the masking and transfer method allowed a fine shape control of the PDA film.

2.3. Embedding of Phospholipids Nanodiscs

The controlled dopamine polymerization only at the conductive areas of the gold substrate offers the opportunity to embed non-conductive molecules or supramolecular structures such as phospholipid bilayers into the thin film, which is of great interest to access nanocomposite functional materials. In this case, the current should not flow at positions, where the non-conductive elements have been placed and PDA polymerization should only occur at the conductive surface areas. Lipid nanodiscs were selected due to their rich functionality and defined dimensions such as the formation of precise nanopores filled with lipids and the opportunity to incorporate membrane proteins into the discs.

Phospholipid nanodiscs were prepared according to a published protocol^[11] using Glycophorin A transmembrane domain (GpAtm) as a model membrane protein. This model protein domain was used in a molar ratio of 1:1 relative to the membrane scaffold protein (MSP) to realize one GpAtm dimer per nanodisc. The nanodiscs were characterized by AFM revealing uniform nanoobjects with discoidal shapes providing a diameter of 10 nm and a height of ≈ 3 nm (Figure 4B). These dimensions correlate well with previous reports.^[11,50] GpAtm incorporation into the nanodiscs was verified using a biotin labeled GpAtm derivative that induces a significant size increase after the addition of streptavidin, which also allows nanodiscs separation during size exclusion chromatography (Figure S9, Supporting Information). Then, the nanodisc solution with a concentration of $1.6 \mu\text{g mL}^{-1}$ was drop cast on a gold substrate, which was prefunctionalized with 3,3'-dithio bis(sulfosuccinimidyl propionate) (DTSSP)^[51] to enhance binding of the nanodiscs to the gold surface (Figure S6, Supporting Information). The nanodiscs adsorbed at the gold surface (Figure S7, Supporting Information) were then embedded into the PDA film

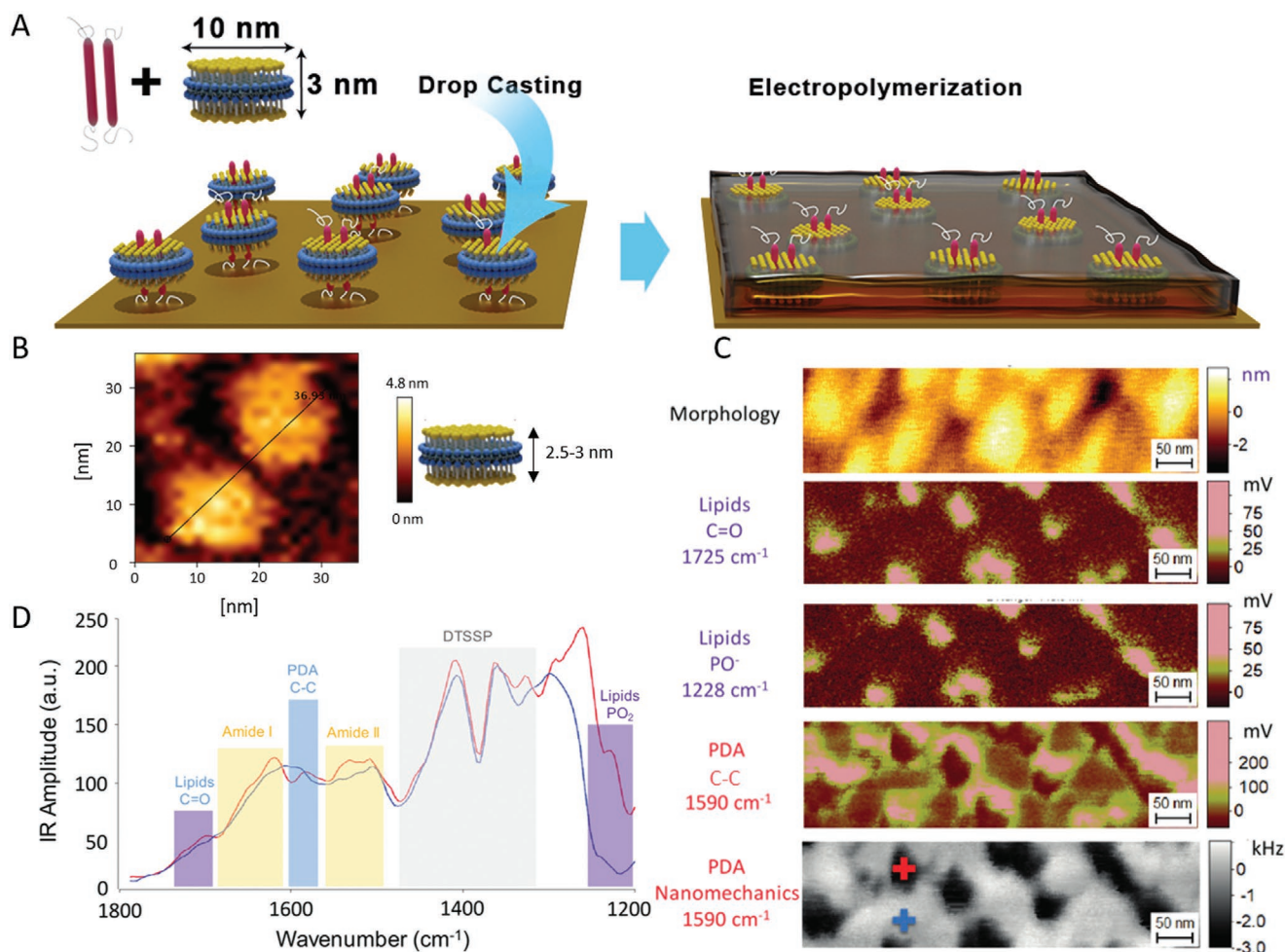


Figure 4. A) Procedure for embedding the nanodiscs with the integrated transmembrane domain of glycoprotein A into the PDA film. B) AFM maps of the nanodiscs. C) AFM maps of the nanodiscs embedded into the PDA film on gold. The red cross indicates where the nanodiscs are present, the blue cross indicates where only PDA is detected. D) IR spectrum of the nanodiscs embedded into the PDA film.

during electropolymerization (Figure 4A). Five CV cycles were performed with a faster scan rate of 0.05 V s⁻¹ yielding sharper peaks in the CV (Figure S8, Supporting Information) to produce a 6 nm film preventing overgrowth of the nanodiscs by the PDA film. AFM-IR was applied to characterize the films to prove the presence of single nanodiscs within the few nanometer thick PDA film with a chemical spatial resolution of ≈10 nm (Figure 4C).

Because of the comparable size of the nanodiscs and the film roughness, as expected, we could not directly identify the nanodiscs by conventional morphology imaging. In order to chemically identify the presence and spatial distribution of the nanodiscs, we imaged the chemical differences of the polymeric PDA matrix and the lipid components of the nanodiscs. As depicted in Figure 2B, PDA has a broad absorption at 1600 cm⁻¹. On the other hand, lipids reveal a typical IR absorption at 1720–1730 cm⁻¹, corresponding to the C=O stretching vibration, and at 1228 cm⁻¹, corresponding to the IR absorption of phospholipids PO₂ groups. We simultaneously acquired nanoscale resolved maps of morphology, nanomechanics and IR absorption of the sample by AFM-IR exploiting gold probes to enhance the electromagnetic field, resonance enhanced

mode and phase-locked loop to increase the sensitivity of the system^[42,52,53] (Figure 4C).

The nanoscale chemical imaging revealed the enhanced absorption of the nanodiscs at the typical IR absorption bands of phospholipids at 1725 and 1228 cm⁻¹ as bright spots in the IR map (Figure 4C). Consequently, at the location of the nanodiscs, one would anticipate a decreased IR absorption related to the diminished local content of PDA. As expected, chemical imaging of the film at 1590 cm⁻¹, corresponding to IR absorption of the C–C ring vibration of PDA, showed a reduced absorption at the locations of the nanodiscs in the IR map. Furthermore, the regions corresponding to the lipids exhibit significantly lower tip-sample frequency of contact resonance, indicating that the lipid–protein nanodiscs have relative lower stiffness than the polymeric PDA film.

We then acquired nanoscale localized spectra from areas close to the nanodiscs and the PDA film (Figure 4C). In good agreement with the chemical imaging, the spectra acquired on the area of the nanodiscs showed an increase of IR absorption at the IR absorption bands of lipids (1720–30 and 1228 cm⁻¹) and of protein amide bands I (1700–1600 cm⁻¹) and II (1580–1500 cm⁻¹)

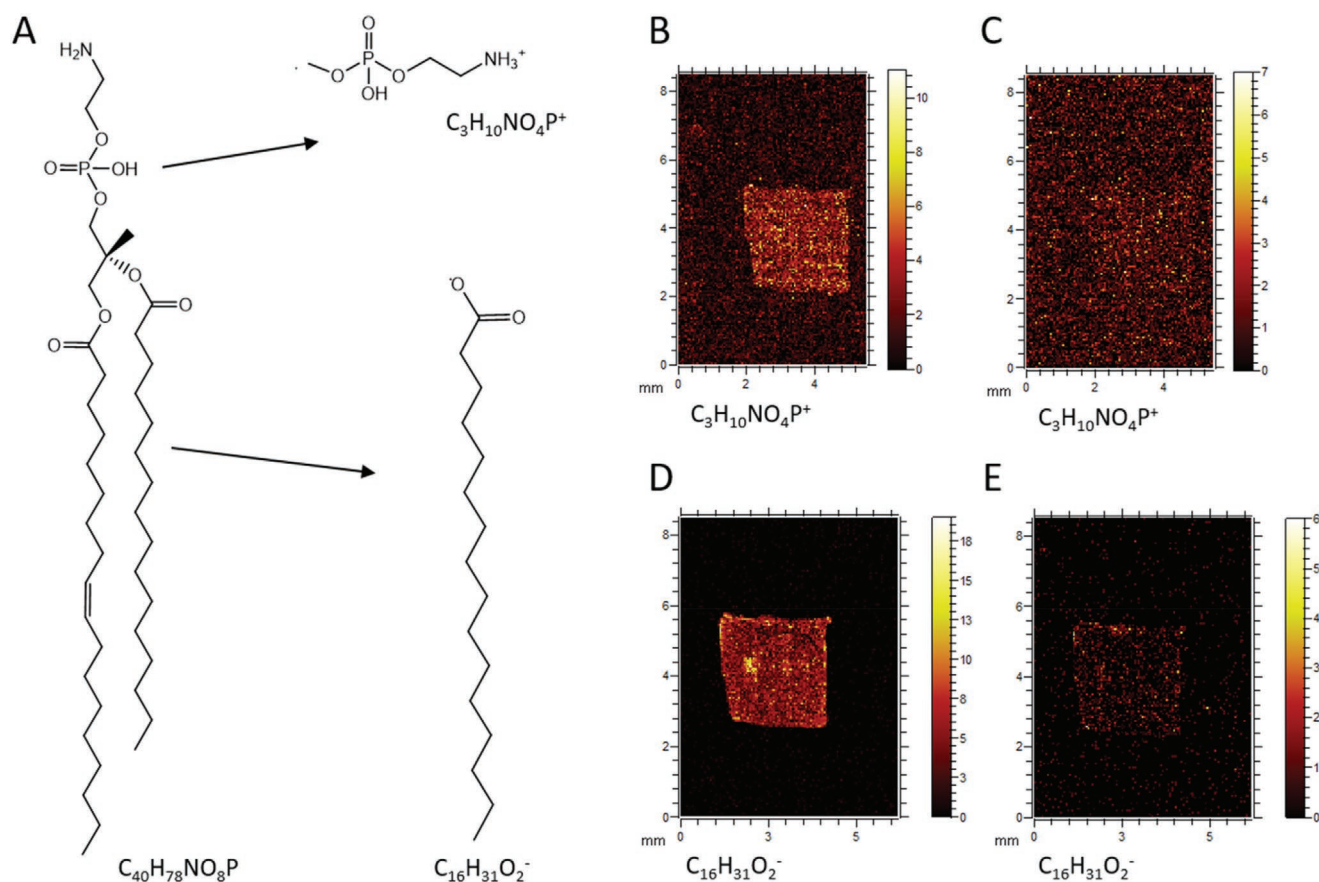


Figure 5. A) Scheme of PE fragmentation process occurring in ToF-SIMS measurements leading to negatively charged fatty acid fragments originating from the non-polar tail and positively charged signals from the head group. B–E) ToF-SIMS imaging signal distributions across the nanodisc functionalized area. B,D) After the nanodisc-immobilization. C,E) After nanodisc-embedding into the PDA film. B) The lateral signal distribution of the PE lipid headgroup fragment C₃H₁₀NO₄P⁺ reveals the highest signal intensity in the central square-shaped nanodisc-deposition area. C) The contrast for the headgroup fragment C₃H₁₀NO₄P⁺ is less pronounced after embedding. However, slightly elevated signal intensities compared to the surrounding area can be observed in the central area. D) The fatty acid fragment C₁₆H₃₁O₂⁻ of the PE lipid matches the expected distribution with high signal intensities in the central area. E) Signal intensities of the fatty acid fragment C₁₆H₃₁O₂⁻ of the PE lipid are reduced compared to the non-embedded sample, but the central square area still shows a notably higher signal intensity.

indicating the presence of the protein in the nanodiscs. In both spectra, there is a dominating contribution arising from the IR absorption of the PDA and of the continuous underlying layer of DTSSP below, which absorbs strongly in the IR at 1400 cm⁻¹ (Figure 4D). These contributions could not be minimized because of the larger size of the AFM tip (≈30 nm) compared to the average radius of the nanodiscs (≈5 nm), thermal diffusion or the long-range penetration depth of the IR light sensing also the underlying DTSSP layer. However, these results clearly indicated that the thin disks were actually embedded within the PDA film.

Time-of-flight secondary ion mass spectrometry (ToF-SIMS) was used to detect the phosphatidylethanolamine (PE) lipids (57.5 w/wt%) from the nanodiscs deposited on the gold surface. The PE molecule consists of a phosphatidylethanolamine headgroup and fatty acid chains. Therefore, fragment signals from both parts of the lipids were expected as shown in Figure 5A. The sample was prepared by masking a square of 2.5 × 2.5 mm² of DTSSP-functionalized gold with PDMS to confine the nanodiscs at the surface. After deposition of the nanodiscs, the sample was rinsed with deionized water and the mask was removed, following

the electropolymerization of a 6 nm thin PDA film. The sample was analyzed by ToF-SIMS imaging before and after the PDA film deposition. In the absence of the PDA film, the PE-related signals were well detectable on the gold substrate, while the signal intensities decreased significantly after PDA film formation. Figure 5B reveals the signal distributions of the positively charged PE headgroup fragment C₃H₁₀NO₄P⁺ in the drop cast nanodiscs area. In Figure 5D, the negatively ionized signal distribution of the fatty acid fragment C₁₆H₃₁O₂⁻ of the PE lipids is shown. Both signal distributions reveal the highest signal intensities in the central square area. Additionally, the fatty acid signals appear more intense compared to the signals of the PE headgroup fragment providing a higher contrast. The colocalization of the intense signals for both, the PE headgroup and the fatty acid, indicates the presence of the nanodiscs on the gold surface.

The PDA film was polymerized after six cycles at 50 mV s⁻¹ on the substrate containing the nanodiscs applying the same setup as above. The signal intensities of the fatty acid- and headgroup-related signals decreased significantly as shown in Figure 5C,E, but they were still detectable. A slightly higher signal intensity

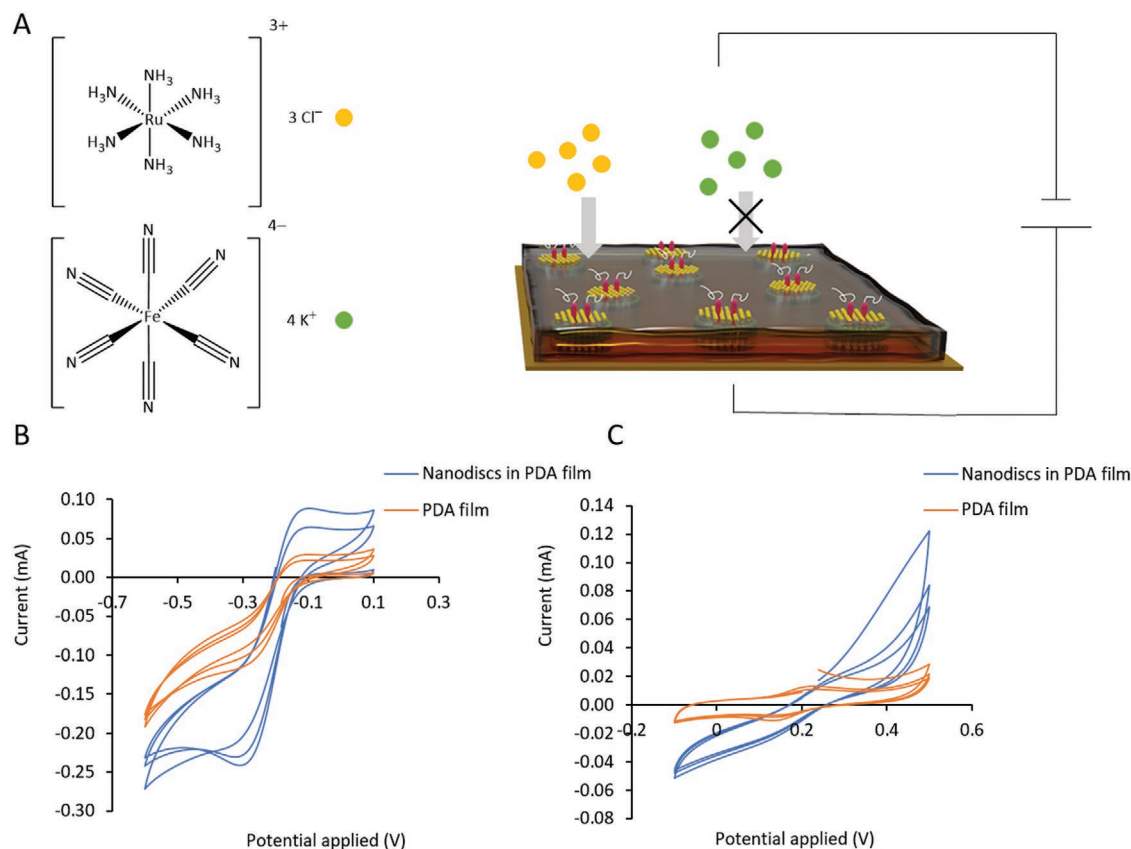


Figure 6. A) Schematic procedure of electrochemical test for ion permeability through PDA and ND film; $\text{Ru}(\text{NH}_3)_6\text{Cl}_3$ represented by yellow circles and potassium ferrocyanide represented by green circles. B–C) Cyclic voltammetry of a 6 nm PDA film with the nanodiscs embedded inside (blue curve) and without the nanodiscs (orange curve) using Ag/AgCl as reference electrode and Pt wire as counter electrode in phosphate buffer pH 7. B) Voltammogram recorded by using $\text{Ru}(\text{NH}_3)_6\text{Cl}_3$ as redox probe sweeping the potential between -0.6 and $+0.1$ V for three cycles. C) Voltammogram recorded by using a 5 mm equal mixture of $\text{K}_3[\text{Fe}(\text{CN})_6]/\text{K}_4[\text{Fe}(\text{CN})_6]$ as redox probe sweeping the potential between -0.1 and $+0.5$ V for three cycles.

relating from $\text{C}_3\text{H}_{10}\text{NO}_4\text{P}^+$ was found in the central square area, where the nanodiscs were deposited suggesting the presence of the lipids bilayers in the PDA film. The intensity of the signals relating to the fatty acid distribution (Figure 5E) was also much lower after embedding the nanodiscs into the PDA film. Nevertheless, a higher signal intensity was observed in the central area, still depicting the square shape from the mask. This indicates that the lipids of the nanodiscs were present within the topmost layers of the PDA surface (<1 nm). The ToF-SIMS experiments indicated that the lipid bilayers were still accessible after embedding, suggesting the formation of channels, which could provide great potential for advanced separations and as cell membrane mimics.

Next, we studied the availability of the nanodisc pores to control ion transport. The ion permeability through ultrathin PDA films on the gold surface with and without the embedded nanodiscs was investigated by cyclic voltammetry as shown in Figure 6A. Ruthenium hexamine chloride, $\text{Ru}(\text{NH}_3)_6\text{Cl}_3$, was used as redox probe due to its positive charge, which would in principle allow permeation through the film due to the introduction of negatively charged phospholipids bilayers. Figure 6B depicts the resulting cyclic voltammetry graphs of the 6 nm polydopamine films with and without the embedded nanodiscs. By applying a potential between -0.6 and $+0.1$ V, the typical oxidation and reduction peaks from $\text{Ru}(\text{NH}_3)_6\text{Cl}_3$ appear at

-0.1 and -0.3 V, respectively, indicating that $\text{Ru}(\text{NH}_3)_6\text{Cl}_3$ reached the gold surface, where it further reacted. Compared to the PDA film without the nanodiscs, the PDA film containing the accessible nanodiscs showed a significantly increased signal for both oxidation and reaction peaks, which was indicative for an enhanced permeability of $\text{Ru}(\text{NH}_3)_6\text{Cl}_3$.

Comparative CV measurements were performed applying $\text{K}_3[\text{Fe}(\text{CN})_6]/\text{K}_4[\text{Fe}(\text{CN})_6]$ as redox couple with negative charge. Figure 6C depicts the cyclic voltammetry graphs using $\text{K}_3[\text{Fe}(\text{CN})_6]/\text{K}_4[\text{Fe}(\text{CN})_6]$ by applying a potential between -0.1 and $+0.5$ V. In both cases, the oxidation and reduction peaks that typically appear at $+0.3$ and $+0.1$ V, respectively, are barely distinguishable indicating a weak permeation of the redox probe through the PDA film to the gold electrode. These results indicated the availability of nanodiscs in the film with accessible pores filled with phospholipids that participated in transport through the PDA film rendering it permeable to positively charged $\text{Ru}(\text{NH}_3)_6\text{Cl}_3$ and much less permeable to $\text{K}_3[\text{Fe}(\text{CN})_6]/\text{K}_4[\text{Fe}(\text{CN})_6]$.

3. Conclusions

Herein, the first ultrathin, freestanding PDA films were prepared by electropolymerization and application of the

sacrificial polymer PVA. Delamination of the PDA film was accomplished in a non-destructive way yielding PDA films with 10–20 nm thickness that were successfully transferred onto various other substrates such as Si, Si₃N₄, glass slide, and nylon. This procedure was scaled conveniently up to 2.5 cm² dimensions and the PDA films revealed outstanding Young moduli of about 12 GPa after applying five and ten polymerization cycles. Moreover, dopamine polymerization could be spatially controlled by applying a non-conducting PDMS mask as well as non-conducting biomolecules. In this way, patterned PDA films were prepared and transferred successfully without deformation. Non-conducting phospholipid nanodiscs containing the transmembrane domain of glycoporphin A were successfully embedded into the PDA film and the shapes of the nanodiscs were retained after electropolymerization. The lipid bilayers in the nanopores remained at the surface of the film and accessible after PDA deposition. Increased permeability of Ru(NH₃)₆·Cl₃ was observed in the presence of the nanopores, whereas only very low permeability for K₃[Fe(CN)₆]/K₄[Fe(CN)₆] was measured for PDA and PDA with nanodiscs.

We believe that the reported procedure solves the long-lasting challenge to fabricate polymeric films with ultrathin geometries,^[12] as well as their transfer to other substrates^[13–16,54] and the incorporation of functional biological entities. Therefore, these ultrathin PDA films could be of great interest in flexible electronics, water purification, separation, and tissue engineering. The presence of protein nanopores within the PDA films provide a unique platform, into which membrane proteins could be integrated, for example, to allow their structure investigations in more native environments. Future work will also focus on elucidating the functionality of the embedded nanopores for, for example, the selective separation of organic molecules, nanopore-based DNA-sequencing, cascade reactions, or sensing.

4. Experimental Section

Gold-coated (1000 Å) microscope slide (Sigma-Aldrich), were cut using a diamond tip.

Phosphate buffer pH 7, 100 mM was prepared using sodium phosphate dibasic anhydrous (99%) and sodium phosphate monobasic (99%) (Sigma-Aldrich) in Milli-Q water. Carbonate buffer pH 10, 100 mM was prepared using sodium bicarbonate (>99.7%) and sodium carbonate (>99.8%) from Sigma-Aldrich, in Milli-Q water. Polyvinyl alcohol 80% hydrolyzed 9–10 kDa Mw (Sigma-Aldrich) was used to prepare the 10 wt% solution in Milli-Q water. Nylon net 60 µm was purchased from Merck. Potassium ferricyanide (99+%) and potassium ferrocyanide trihydrate (99+%) were bought from Acros Organics. DTSSP (3,3'-dithiobis(sulfosuccinimidyl propionate) was purchased from (Chem Cruz). Sodium dihydrogenphosphate was obtained from Sigma-Aldrich and potassium hydrogen phosphate from Appli Chem.

Film Preparation: Electropolymerization and cyclic voltammetry experiments were performed using a Metrohm Autolab Nseries potentiostat (AUTOLAB PGSTAT 204) with a standard three electrode configuration. A gold covered glass microscope slide was used as the working electrode, a Ag/AgCl, 3 M KCl as the reference electrode, and gold wire as the counter electrode for film preparation while a platinum wire for CV experiments. All reactions were performed in a 35 mL electrochemical cell (Metrohm), in air atmosphere and at room

temperature. Pre-treatment of gold working electrode was performed by 10 min in Ar plasma cleaning at the pressure of 6 mbar.

Gold was used as substrate for electrodeposition of PDA due to its inertness, excellent conductivity, and low surface roughness. After cleaning in argon plasma, the gold substrate was immersed in a 1 mg mL⁻¹ solution of dopamine hydrochloride dissolved in 100 mM phosphate buffer at pH 7.0. A potential was applied and cycled from +500 mV to –500 mV with a scan rate 0.01 V s⁻¹ to induce dopamine polymerization at the interface. The film thickness was controlled by the number of cycles as determined by AFM (Park NX20).

Film Transfer Procedure: The PVA/PDA film was placed gently on the water surface with the polydopamine side facing the liquid side and after a couple of minutes, it could be noticed that the PVA layer expanded and dissolved leaving only the PDA film floating on water. Once the film floated on water, it could be fished from the bottom with a support like a nylon mesh leading in this way to a freestanding polydopamine film. Then the sample was washed in water for 1 h and in 45 °C water for 1 h to completely remove the PVA and subsequently dried at room temperature for 1 h. SEM Images were acquired using LEO Gemini 1530 by attaching the sample with double side tape on the sample holder.

Deposition of Nanodiscs: In general, 10 µL of a 16 µg mL⁻¹ concentrated solution of nanodiscs in PBS (137 mM NaCl, 2.7 mM KCl, 10 mM Na₂HPO₄, 1.8 mM KH₂PO₄) was used and incubated on the substrates under different conditions varying in time and temperature. Gold was cleaned with argon plasma for 10 min at 6 mmbar before being used.

Moreover, the nanodiscs were attached to gold surface by using the crosslinker DTSSP. As a cross-linker, DTSSP offers the possibility for a covalent linkage of the nanodiscs MSP to the gold surface, since it creates a self-assembled monolayer (SAM-layer) on the gold surface by chemisorption using interactions between gold and the disulphide linkage of DTSSP. In a second reaction step primary amines of the MSP lysine residues can react with the functional NHS-ester of DTSSP to covalently bind the nanodiscs to the gold surface (Figure S6, Supporting Information).

For the formation of a SAM-layer on gold 200 µL of a 5 mM DTSSP in PBS (137 mM NaCl, 2.7 mM KCl, 10 mM Na₂HPO₄, 1.8 mM KH₂PO₄) solution was attached to the gold surface and incubated at several conditions. After washing with 2 mL PBS 10 µL of a 16 µg mL⁻¹ concentrated solution of Nanodiscs in PBS was added to the gold slide and incubated at 4 °C for 24 h. The gold slides were washed with 2 mL PBS and dried with nitrogen. The six cycles polydopamine film was then performed on the gold with the nanodiscs applying a scan rate of 50 mV s⁻¹ and the CV is shown in Figure S7, Supporting Information.

Supporting Information

Supporting Information is available from the Wiley Online Library or from the author.

Acknowledgements

The authors acknowledge support by the BMBF (Biotechnologie 2020 + initiative, “Selekomm” project). This work received funding from the Deutsche Forschungsgemeinschaft (DFG, German Research Foundation) under the Collaborative Research Center (CRC) Transregio 234 (No. 407426226, B04). T.W., K.W. and T.M. are grateful for the support from the Marie Curie ITN BORGES (No. 813863). T.W. acknowledges support from ERC Synergy Grant BioQ (No. 319130); G.F. and K.W. acknowledge support from ERC Ad G SmartPhon (No. 694977). Open Access funding provided by the Max Planck Society is acknowledged. The authors also thank Katharina Maisenbacher for support with drawing of the TOC figure.

Conflict of Interest

The authors declare no conflict of interest.

Keywords

freestanding ultrathin films, glycophorin A, membrane mimics, nanodiscs, polydopamine

Received: January 14, 2020

Published online: March 23, 2020

- [1] C. Lang, D. Ye, W. Song, C. Yao, Y. M. Tu, C. Capparelli, J. A. LaNasa, M. A. Hickner, E. W. Gomez, E. D. Gomez, R. J. Hickey, M. Kumar, *ACS Nano* **2019**, *13*, 8292.
- [2] a) Y. Xu, J. Fei, G. Li, T. Yuan, X. Xu, J. Li, *Angew. Chem., Int. Ed.* **2019**, *58*, 5572; b) *Angew. Chem.* **2019**, *131*, 5628.
- [3] E. Diamanti, E. Gutierrez-Pineda, N. Politakos, P. Andreozzi, M. J. Rodriguez-Presa, W. Knoll, O. Azzaroni, C. A. Gervasi, S. E. Moya, *Soft Matter* **2017**, *13*, 8922.
- [4] P. S. Zhong, T.-S. Chung, K. Jeyaseelan, A. Armugam, *J. Membr. Sci.* **2012**, *407–408*, 27.
- [5] C. G. Palivan, O. Fischer-Onaca, M. Delcea, F. Itel, W. Meier, *Chem. Soc. Rev.* **2012**, *41*, 2800.
- [6] S. Howorka, *Nat. Nanotechnol.* **2017**, *12*, 619.
- [7] Y.-X. Shen, P. O. Saboe, I. T. Sines, M. Erbakan, M. Kumar, *J. Membr. Sci.* **2014**, *454*, 359.
- [8] Y. Ge, X. Shen, H. Cao, L. Jin, J. Shang, Y. Wang, T. Pan, Y. Yang, Z. Qi, *Langmuir* **2019**, *35*, 7824.
- [9] I. G. Denisov, S. G. Sligar, *Chem. Rev.* **2017**, *117*, 4669.
- [10] M. E. Zoghbi, G. A. Altenberg, *Nanotechnol. Rev.* **2017**, *6*, 33.
- [11] I. G. Denisov, Y. V. Grinkova, A. A. Lazarides, S. G. Sligar, *J. Am. Chem. Soc.* **2004**, *126*, 3477.
- [12] H. Zhang, Y. Liu, C. Yang, L. Xiang, Y. Hu, L. M. Peng, *Adv. Mater.* **2018**, *30*, 1804715.
- [13] Z. Zheng, C. T. Nottbohm, A. Turchanin, H. Muzik, A. Beyer, M. Heilemann, M. Sauer, A. Golzhauser, *Angew. Chem., Int. Ed.* **2010**, *49*, 8493.
- [14] X. D. Chen, Z.-B. Liu, C.-Y. Zheng, F. Xing, X.-Q. Yan, Y. Chen, J.-G. Tian, *Carbon* **2013**, *56*, 271.
- [15] Z. Jiang, S. Karan, A. G. Livingston, *Adv. Mater.* **2018**, *30*, 1870107.
- [16] Y. Liu, K. Ai, L. Lu, *Chem. Rev.* **2014**, *114*, 5057.
- [17] H. Lee, B. P. Lee, P. B. Messersmith, *Nature* **2007**, *448*, 338.
- [18] A. Neveshkin, P. Citak, V. Ball, M. Winterhalter, *Langmuir* **2017**, *33*, 7256.
- [19] S. Sieste, T. Mack, C. V. Synatschke, C. Schilling, C. Meyer Zu Reckendorf, L. Pendi, S. Harvey, F. S. Ruggeri, T. P. J. Knowles, C. Meier, D. Y. W. Ng, T. Weil, B. Knoll, *Adv. Healthcare Mater.* **2018**, *7*, 1701485.
- [20] A. GhavamiNejad, L. E. Aguilar, R. B. Ambade, S.-H. Lee, C. H. Park, C. S. Kim, *Colloids Interface Sci. Commun.* **2015**, *6*, 5.
- [21] X. Han, F. Tang, Z. Jin, *RSC Adv.* **2018**, *8*, 18347.
- [22] F. Ponzio, P. Payamyar, A. Schneider, M. Winterhalter, J. Bour, F. Addiego, M. P. Krafft, J. Hemmerle, V. Ball, *J. Phys. Chem. Lett.* **2014**, *5*, 3436.
- [23] L. Zhang, P. Xiao, W. Lu, J. Zhang, J. Gu, Y. Huang, T. Chen, *Adv. Mater. Interfaces* **2016**, *3*, 1600170.
- [24] H. C. Yang, W. Xu, Y. Du, J. Wu, Z.-K. Xu, *RSC Adv.* **2014**, *4*, 45415.
- [25] S. Hong, C. F. Schaber, K. Denning, E. Appel, S. N. Gorb, H. Lee, *Adv. Mater.* **2014**, *26*, 7581.
- [26] F. Ponzio, V. Le Houerou, S. Zafeiratos, C. Gauthier, T. Garnier, L. JERRY, V. Ball, *Langmuir* **2017**, *33*, 2420.
- [27] D. Hafner, L. Ziegler, M. Ichwan, T. Zhang, M. Schneider, M. Schiffrmann, C. Thomas, K. Hinrichs, R. Jordan, I. Amin, *Adv. Mater.* **2016**, *28*, 1489.
- [28] B. Stöckle, D. Y.W. Ng, C. Meier, T. Paust, F. Bischoff, T. Diemant, R. J. Behm, K.-E. Gottschalk, U. Ziener, T. Weil, *Macromol. Symp.* **2014**, *346*, 73.
- [29] J. L. Wang, B. C. Li, Z. J. Li, K. F. Ren, L. J. Jin, S. M. Zhang, H. Chang, Y. X. Sun, J. Ji, *Biomaterials* **2014**, *35*, 7679.
- [30] J. Lin, S. Daboss, D. Blaimer, C. Kranz, *Nanomaterials* **2019**, *9*, 242.
- [31] L. Klosterman, Z. Ahmad, V. Viswanathan, C. J. Bettinger, *Adv. Mater. Interfaces* **2017**, *4*, 1700041.
- [32] H. Furthmayr, V. T. Marchesi, *Biochemistry* **1976**, *15*, 1137.
- [33] Y. Li, M. Liu, C. Xiang, Q. Xie, S. Yao, *Thin Solid Films* **2006**, *497*, 270.
- [34] R. A. Zangmeister, T. A. Morris, M. J. Tarlov, *Langmuir* **2013**, *29*, 8619.
- [35] F. Greco, A. Zucca, S. Taccola, A. Mencias, T. Fujie, H. Haniuda, S. Takeoka, P. Dario, V. Mattoli, *Soft Matter* **2011**, *7*, 10642.
- [36] W. Yang, C. Liu, Y. Chen, *Langmuir* **2018**, *34*, 3565.
- [37] R. Holze, *Phys. Chem. Chem. Phys.* **2015**, *17*, 21364.
- [38] M. Rueda, F. Prieto, J. Álvarez-Malmagro, A. Rodes, *Electrochem. Commun.* **2013**, *35*, 53.
- [39] R. Avila-Flores, R. A. Medellin, *J. Mammal.* **2004**, *85*, 675.
- [40] F. S. Ruggeri, J. Habchi, A. Cerreta, G. Dietler, *Curr. Pharm. Des.* **2016**, *22*, 3950.
- [41] F. S. Ruggeri, G. Longo, S. Faggiano, E. Lipiec, A. Pastore, G. Dietler, *Nat. Commun.* **2015**, *6*, 7831.
- [42] F. S. Ruggeri, S. Vieweg, U. Cendrowska, G. Longo, A. Chiki, H. A. Lashuel, G. Dietler, *Sci. Rep.* **2016**, *6*, 31155.
- [43] E. Lipiec, F. S. Ruggeri, C. Benadiba, A. M. Borkowska, J. D. Kobierski, J. Miszczyk, B. R. Wood, G. B. Deacon, A. Kulik, G. Dietler, W. M. Kwiatek, *Nucleic Acids Res.* **2019**, *47*, e108.
- [44] Y. C. Lin, C. C. Lu, C. H. Yeh, C. Jin, K. Suenaga, P. W. Chiu, *Nano Lett.* **2012**, *12*, 414.
- [45] S. H. Hwang, D. Kang, R. S. Ruoff, H. S. Shin, Y.-B. Park, *ACS Nano* **2014**, *8*, 6739.
- [46] B. Graczykowski, M. Sledzinska, M. Placidi, D. Saleta Reig, M. Kasprzak, F. Alzina, C. M. Sotomayor Torres, *Nano Lett.* **2017**, *17*, 7647.
- [47] A. H. Koch, G. Lévêque, S. Harms, K. Jaskiewicz, M. Bernhardt, A. Henkel, C. Sönnichsen, K. Landfester, G. Fytas, *Nano Lett.* **2014**, *14*, 4138.
- [48] X. Zhang, C. Neumann, P. Angelova, A. Beyer, A. Golzhauser, *Langmuir* **2014**, *30*, 8221.
- [49] S. H. Baxamusa, M. Stadermann, C. Aracne-Ruddle, A. J. Nelson, M. Chea, S. Li, K. Youngblood, T. I. Suratwala, *Langmuir* **2014**, *30*, 5126.
- [50] T. H. Bayburt, Y. V. Grinkova, S. G. Sligar, *Nano Lett.* **2002**, *2*, 853.
- [51] S. H. Tark, A. Das, S. Sligar, V. P. Dravid, *Nanotechnology* **2010**, *21*, 435502.
- [52] S. Qamar, G. Wang, S. J. Randle, F. S. Ruggeri, J. A. Varela, J. Q. Lin, E. C. Phillips, A. Miyashita, D. Williams, F. Strohl, W. Meadows, R. Ferry, V. J. Dardov, G. G. Tartaglia, L. A. Farrer, G. S. Kaminski Schierle, C. F. Kaminski, C. E. Holt, P. E. Fraser, G. Schmitt-Ulms, D. Klennerman, T. Knowles, M. Vendruscolo, P. St George-Hyslop, *Cell* **2018**, *173*, 720.
- [53] F. S. Ruggeri, T. Šneideris, S. Chia, M. Vendruscolo, T. P. Knowles, *J. Visualized Exp.* **2019**, *151*, e60108.
- [54] M. M. Pérez-Madrugal, E. Armelin, J. Puiggalí, C. Alemán, *J. Mater. Chem. B* **2015**, *3*, 5904.